Valley symmetry breaking and gap tuning in graphene by spin doping

New Journal of Physics
The open-access journal for physics

Valley symmetry breaking and gap tuning in graphene by spin doping

Antonio Hill, Andreas Sinner and Klaus Ziegler[1]
Institut für Physik, Universität Augsburg, Germany
E-mail: klaus.ziegler@physik.uni-augsburg.de

New Journal of Physics **13** (2011) 035023 (14pp)
Received 18 November 2010
Published 29 March 2011
Online at http://www.njp.org/
doi:10.1088/1367-2630/13/3/035023

Abstract. We study graphene with an adsorbed spin texture, where the localized spins create a periodic magnetic flux. The latter produces gaps in the graphene spectrum and breaks the valley symmetry. The resulting effective electronic model, which is similar to Haldane's periodic flux model, allows us to tune the gap of one valley independently from that of the other valley. This leads to the formation of two Hall plateaux and a quantum Hall transition. We discuss the density of states, optical longitudinal and Hall conductivities for nonzero frequencies and nonzero temperatures. A robust logarithmic singularity appears in the Hall conductivity when the frequency of the external field agrees with the width of the gap.

Contents

[1] Author to whom any correspondence should be addressed.

1. Introduction

Transport properties of neutral graphene are characterized by a semimetallic behavior with a point-like Fermi surface at two valleys. This can be changed by external electric fields in gated graphene to a more classical transport with a circular Fermi surface or by an external magnetic field that opens gaps in the spectrum [1, 2]. The latter leads to the formation of Hall plateaux in the Hall conductivity. Another possibility is to introduce a gap either by chemical doping (e.g. with hydrogen [3]) or in bilayer graphene with a double gate [4]–[9]. Chemical doping is an interesting direction for modifying graphene because it leads to a rich field with new properties. Although a standard technique for semiconductors, it has been applied to graphene only recently ([3], [9]–[15]). As a special case of chemical doping, one can use atoms that carry a spin to create a spin texture on graphene. These localized spins alter the transport properties of graphene significantly. This will be discussed in this paper.

The quantum Hall effect in graphene was observed in a number of experiments, cf [1, 2]. It is usually associated with the presence of an external homogeneous magnetic field that separates the electronic spectrum into Landau levels. Without an external magnetic field, each valley of the honeycomb spectrum provides a quantum Hall step [17]. However, the system is time-reversal invariant. This implies that the Hall conductivity vanishes, since the contribution of the two valleys to the Hall conductivity cancel each other. A magnetic flux, however, can cure this problem by breaking the time-reversal invariance. A possible way to observe the quantum Hall effect is by introducing a periodic magnetic flux. This was suggested by Haldane [16]: a staggered magnetic flux, in combination with nearest- and next-nearest neighbor hopping and a staggered potential on the honeycomb lattice, creates two Hall plateaux with Hall conductivities $\sigma_{xy} = \pm e^2/h$. The periodic magnetic field leads to a staggered flux with zero net flux in each unit cell. It affects the hopping matrix elements by creating a phase factor that enables us to change the signs of the Hall conductivities of each node independently by changing the magnetic field strength. The effects of the staggered potential and staggered magnetic flux can also be understood in terms of symmetry breaking: the Brillouin zone (BZ) has a sixfold energetic degeneracy due to the vanishing energy at the corners of its hexagonal structure. A staggered potential breaks the inversion symmetry [16, 17] but preserves the sixfold energetic degeneracy, because all six corners acquire the same gap. The staggered magnetic flux, however, reduces the sixfold degeneracy to a threefold degeneracy (i.e. it provides inter-valley symmetry breaking) because it affects the gap of the two Dirac nodes differently.

The importance of sublattice and inter-valley symmetry breaking in graphene for applications has been widely recognized. Recently, the effect of the broken inversion symmetry in graphene was addressed in the context of topological [18] and anomalous thermoelectric [19] transport, as well as valley-dependent optoelectronics [20].

Systematic doping of graphene with noncarbon atoms has become a realistic opportunity to modify substantially the properties of the material ([3], [21]–[23]). A particular case is doping with atoms that carry a spin. Then the spin of the itinerant electrons interact with the localized spin of the noncarbon atoms. This has two effects: (i) the hopping rate of the itinerant electrons is modified and depends on the spin orientation; and (ii) the coupling between the localized spins is affected by the interaction with the itinerant electrons, leading to a renormalized interaction between the localized spins. The latter is known as double-exchange interaction [24]–[26] in contrast to the usual exchange interaction of itinerant electrons. While the exchange interaction supports antiferromagnetic order, the double-exchange interaction

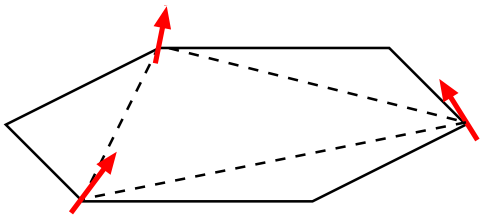

Figure 1. Spinor atoms on a unit cell of graphene. Tilted spin textures can provide an effective staggered magnetic flux [27]–[29].

favors ferromagnetic ordering. This is because the itinerant electrons are blocked by the antiferromagnetic order of the localized spins, whereas they can move in a ferromagnetically ordered background. Thus ferromagnetic order is favored, since the motion of the itinerant electrons lowers the energy of the ferromagnetic system. Then the competition between exchange and double-exchange interaction creates spin configurations with tilted spins [25, 26].

In this paper, we propose a model that is based on a honeycomb lattice, where one sublattice is occupied by localized spins. This leads to an effective hopping parameter with a Berry phase and reflects the equivalence of the spin texture with an effective periodic magnetic flux in the tight-binding model. It is similar but slightly different from Haldane's periodic flux model. The inter-valley symmetry is lifted by introducing only a next-nearest-neighbor hopping on one sublattice and a staggered magnetic flux. This choice is motivated by the fact that graphene on a substrate can adsorb atoms only on one side. In this case, the adsorbed atoms occupy only next-nearest neighbor-sites on the honeycomb lattice, i.e. they occupy one sublattice. Such a possibility was experimentally observed for hydrogen on graphene [3]. As a result, the adsorbed atoms modify the overlap integrals on their sublattice and may even create an additional next-nearest-neighbor hopping. Moreover, if the adsorbed atoms have a magnetic moment, these moments can form a localized spin texture due to double exchange [24]–[26]. It is known that such spin structures provide an effective Berry phase for the electron hopping rate [27]–[29]. The latter has the same effect as a periodic (staggered) flux, where the flux depends on the tilting angle of the localized spins (figures 1 and 2).

2. The model: electronic hopping on a spin texture

We consider localized $S = 1/2$ spins on a graphene lattice, where the latter is assumed to be flat. As a reference system, we choose a basis of eigenspins oriented in the z-direction with the lattice in the x–y-plane. In other words, the z-component of the localized spin 1/2 operator satisfies $S^z|\pm\rangle = \pm|\pm\rangle$. In terms of Pauli matrices $\vec{\sigma} = (\sigma_x, \sigma_y, \sigma_z)$, this reads

$$\sigma_z \mathbf{s}_\pm = \pm \mathbf{s}_\pm, \tag{1}$$

with the two-component spinor basis $\{\mathbf{s}_+, \mathbf{s}_-\}$. In general, a spin state can have a local orientation, such that it is an eigenstate to $\vec{n}_j \cdot \vec{\sigma}$ with the three-dimensional (3D) unit vector $\vec{n}_j = (\sin\theta\cos\phi,\ \sin\theta\sin\phi,\ \cos\theta)$. The matrix of the spin operator $\vec{n}_j \cdot \vec{\sigma}$ reads in the z-oriented basis

$$\vec{n}_j \cdot \vec{\sigma} = \begin{pmatrix} \cos\theta_j & \mathrm{e}^{\mathrm{i}\phi_j}\sin\theta_j \\ \mathrm{e}^{\mathrm{i}\phi_j}\sin\theta_j & -\cos\theta_j \end{pmatrix},$$

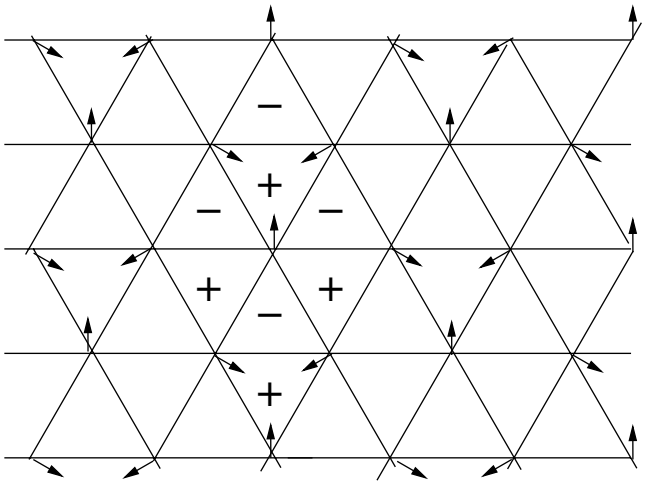

Figure 2. Spin texture on the triangular sublattice with fixed tilting angles (all x–y projected spins have the same length) and x–y rotation angels with multiples of $2\pi/3$. The + (–) signs indicate a positive (negative) magnetic flux through the corresponding (up or down) triangle, whose value is determined by equation (4).

and

$$\mathbf{s}_j = \vec{n}_j \cdot \vec{\sigma}\,\mathbf{s}_+ = \mathrm{e}^{\mathrm{i}b_j} \begin{pmatrix} \cos\theta_j \\ \mathrm{e}^{\mathrm{i}\phi_j}\sin\theta_j \end{pmatrix}.$$

Here the tilting angle θ_j and the x–y rotation angle ϕ_j refer to the change in the quantization direction, relative to the spin state $\mathbf{s}_+$.

Then the electronic Hamiltonian on a honeycomb lattice must describe the interaction of the electronic spin with the localized spins. This leads to a spin-dependent hopping amplitude [27]–[29],

$$\mathcal{H} = \sum_{<i,j>} H_{ij} c_i^\dagger c_j + \mathrm{h.c.}, \tag{2}$$

with

$$H_{ij} = t\mathbf{s}_i \cdot \mathbf{s}_j = t\mathrm{e}^{\mathrm{i}a_{ij}} \cos(\theta_{ij}/2), \tag{3}$$

and electronic creation (annihilation) operators $c_i^\dagger$ (c_j). The Berry phase a_{ij} is given as [29]

$$\sin a_{ij} = -\frac{\sin(\theta_i/2)\sin(\theta_j/2)\sin(\phi_i - \phi_j)}{\cos(\theta_{ij}/2)}, \tag{4}$$

which implies $a_{ij} = -a_{ji}$. (It should be noticed that relation (4) means that a_{ij} is the solid angle spanned by $\mathbf{s}_i$, $\mathbf{s}_j$ and the z-axis [29].) The phase a_{ij} vanishes for vanishing tilting angles θ_i, θ_j (i.e. for ferro- or antiferromagnetic states) and for $\phi_i = \phi_j$ (i.e. when the spin projections on the x–y-plane are parallel. Equation (3) gives us the general expression for the hopping of the electrons in graphene with an additional spin texture, where the latter is characterized by the tilting angles and x–y rotation angles. If we assume a specific configuration of localized spins, the corresponding quantization axis of the spin $\mathbf{s}_j$ is fixed by the angles θ_j and ϕ_j. A special case, where all angles θ_{ij} between next-nearest-neighbor spins and all tilting angles θ_j are equal (except for an irrelevant sign change of θ_{ij} for different pairs i, j), is depicted in figure 2.

This is similar to the situation on the Kagomé lattice in [29]. Moreover, the angles ϕ_j are rotating by $2\pi/3$ on the lattice such that their differences in the expression of the phase a_{ij} in equation (4) are $\pm 2\pi/3$ for next-nearest neighbors. This implies a global renormalization of the hopping rate $t \to t\cos\theta_{ij}$ and a Berry phase that changes only its sign from lattice bond to lattice bond.

2.1. The tight-binding model on the honeycomb lattice

We begin with the tight-binding Hamiltonian of monolayer graphene (i.e. for a honeycomb lattice) and return to the effect of the spin texture later. Then in Fourier space, we can write for the Hamiltonian matrix in sublattice representation

$$H = h_1\sigma_1 + h_2\sigma_2 + h_3\sigma_3, \tag{5}$$

where the off-diagonal Pauli matrices describe the hopping between the two sublattices. The diagonal Pauli matrix term with h_3 describes processes on the same sublattice that can include next-nearest-neighbor tunneling. The eigenvalues of the Hamiltonian are

$$E_\pm = \pm E_k = \pm\sqrt{h_1^2 + h_2^2 + h_3^2}. \tag{6}$$

Specifically for the honeycomb lattice, we have for the nearest-neighbor terms

$$h_1 = -t\sum_{i=1}^{3}\cos(\mathbf{a}_i\cdot\mathbf{k}), \quad h_2 = -t\sum_{i=1}^{3}\sin(\mathbf{a}_i\cdot\mathbf{k}), \tag{7}$$

with the basis vectors of the honeycomb lattice $\mathbf{a}_i$ given by

$$\mathbf{a}_1 = a\,(0,-1)\,, \quad \mathbf{a}_{2,3} = \frac{a}{2}\left(\pm\sqrt{3},1\right), \tag{8}$$

where a denotes the lattice constant. In the absence of a gap, i.e. for $h_3 = 0$, the spectrum defined in equation (6) vanishes at nodal points whose positions in the Fourier space are given by the vectors

$$\mathbf{b}_1^\pm = \frac{4\pi}{3\sqrt{3}a}\,(\pm 1,0)\,, \quad \mathbf{b}_2^\pm = \frac{2\pi}{3\sqrt{3}a}\left(-1,\pm\sqrt{3}\right), \quad \mathbf{b}_3^\pm = \frac{2\pi}{3\sqrt{3}a}\left(1,\pm\sqrt{3}\right). \tag{9}$$

Assuming a uniform gap, i.e. $h_3 = m$, the Hamiltonian defined in equation (5) can be approximated in the vicinity of the nodal points by the Hamiltonian of a massive Dirac fermion

$$H \approx vk_1\sigma_1 + vk_2\sigma_2 + m\sigma_3, \tag{10}$$

where $v = \sqrt{3}ta/2 = 1$ denotes the Fermi velocity of electrons. With this, the eigenvalues read

$$E_\pm = \pm E_k \approx \pm\sqrt{k^2 + m^2}. \tag{11}$$

Now we include the spin texture, described by the modified hopping term of equation (3), by the phase variable $\phi_{\mathbf{r},\mathbf{r}'}$ which is the Berry phase of equation (4). Using a spin texture, as shown in figure 2, we obtain a Berry phase ϕ, which is the same for all three next-nearest-neighbor vectors $\mathbf{c}_j$ ($j = 1, 2, 3$ (cf figure 3)),

$$\mathbf{c}_1 = \sqrt{3}a\,(1,0)\,, \quad \mathbf{c}_{2,3} = \frac{\sqrt{3}a}{2}\left(-1,\pm\sqrt{3}\right), \tag{12}$$

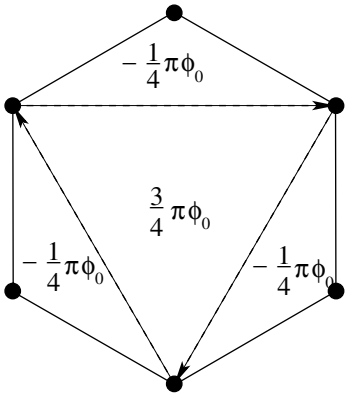

Figure 3. Magnetic flux through the graphene unit cell corresponding to the potential equation (14). Arrows indicate second-neighbor hopping processes and $\phi_0 = h/e$ is the flux quantum.

because the tilting angle is fixed and the x–y rotation angle of the spins is $\pm 2\pi/3$ between next-nearest-neighbor sites. Then the next-nearest-neighbor hopping term reads

$$\chi_{\mathbf{r},\mathbf{r}'} = t' \sum_{j=1}^{3} \left(\mathrm{e}^{-\mathrm{i}\phi} \delta_{\mathbf{r},\mathbf{r}'-\mathbf{c}_j} + \mathrm{e}^{\mathrm{i}\phi} \delta_{\mathbf{r},\mathbf{r}'+\mathbf{c}_j} \right), \tag{13}$$

where t' is the renormalized hopping parameter of equation (3). This hopping term is combined with a uniform gap to give in real space with sublattice co-ordinates $\mathbf{r}$

$$h_{3;\mathbf{r},\mathbf{r}'} = M\ \delta_{\mathbf{r},\mathbf{r}'} + \chi_{\mathbf{r},\mathbf{r}'}, \tag{14}$$

for the third term in equation (5). For the diagonal term, M represents a potential contribution of the doping atoms on the sublattice (i.e. there is a potential difference of $2M$ between the two sublattices) and t' is the contribution of the doping atoms on the next-nearest-neighbor hopping term. After Fourier transformation, we obtain h_3

$$h_3 = M + \chi_{\mathbf{k}} = M + 2t' \sum_{i=1}^{3} \cos\left(\mathbf{c}_i \cdot \mathbf{k} - \phi\right). \tag{15}$$

The term $h_3\sigma_3$ in H of equation (5) opens a gap in the dispersion $\sqrt{h_1^2 + h_2^2 + h_3^2}$ if it is nonzero at the nodal points (valleys) of $\sqrt{h_1^2 + h_2^2}$. Since h_3 is also $\mathbf{k}$ dependent, it can vary the gap independently for the two valleys. It can be adjusted such that the gap parameters have different signs or the gap vanishes at one valley but provides a gap at the other valley. For instance, with $\phi = -\pi/4$ (according to the relation of equation (4), this corresponds to a spin-tilting angle $\theta \approx 1.365$ in figure 2) and $M = 3t'(1+\sqrt{3})/\sqrt{2}$ this term vanishes at the nodal points $\mathbf{b}_1^+$ and $\mathbf{b}_2^\pm$ and remains nonzero at the nodal points $\mathbf{b}_1^-$ and $\mathbf{b}_3^\pm$. The magnetic flux through a unit cell is shown in figure 3 and the related spectrum is presented in figure 4.

This model is similar to the periodic flux model introduced by Haldane [16]. However, the spin texture leads to some differences. In table 1, we compare the gap-opening term h_3 of the spin-texture model with the corresponding term in Haldane's model.

Table 1. Comparison of Haldane's model with our model in terms of the symmetry-breaking quantity h_3. The vector $\mathbf{c}_j$ connects next-nearest-neighbor sites. The summation runs either over both sublattices ($\sum_j^{AB}$) or only over sublattice A ($\sum_j^{A}$). The definition of the variables of Haldane's model are those of [16].

	Haldane's model	Spin-texture model
h_3:	$M - \chi'_{\mathbf{k}}$	$M + \chi_{\mathbf{k}}$
$\chi'_{\mathbf{k}}$:	$2t_2 \sin\phi \sum_j^{AB} \sin(\mathbf{k}\cdot\mathbf{c}_j)$	$2t' \sum_j^{A} \cos(\mathbf{k}\cdot\mathbf{c}_j - \phi)$

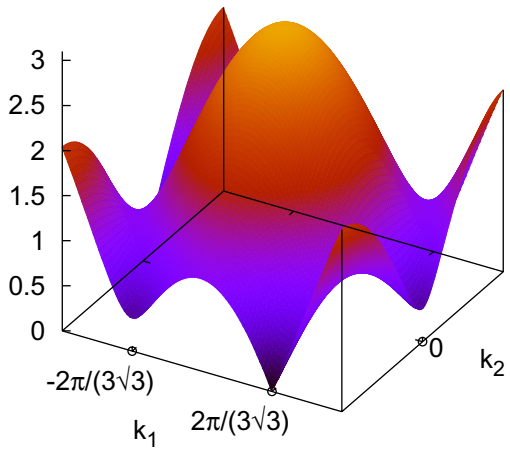

Figure 4. Upper band of the full spectrum of the tight-binding Hamiltonian with the nonuniform gap defined in equations (7) and (15).

Below we will examine how the broken valley symmetry affects the transport properties. For this purpose, we focus on $\phi = -\pi/4$ and compare the results with gapless graphene ($M = t' = 0$) and with graphene with uniform gap ($M \neq 0$, $t' = 0$).

3. The density of states (DOS)

The density of states (DOS) is the imaginary part of the single-particle Green's function

$$\rho(E) = -\mathrm{Im}\,\mathrm{Tr}_2\,\frac{1}{\pi}\int_{\mathrm{BZ}}\left(H - E + \mathrm{i}0^+\right)^{-1}\frac{\mathrm{d}^2k}{\Omega_{\mathrm{BZ}}}. \tag{16}$$

Here, the operator Tr_2 acts on the pseudospinor space and the momentum integral is taken over the BZ of the honeycomb lattice, whereas Ω_{BZ} denotes its volume.

For the low-energy model of equation (10), the DOS can be evaluated explicitly when the integration over the BZ is replaced by one over a circular area with radius λ,

$$\rho(E) = \mathrm{Im}\int_0^{\lambda}\left(\frac{1}{E - E_k - i0^+} + \frac{1}{E + E_k - i0^+}\right)k\frac{\mathrm{d}k}{2\pi^2}, \tag{17}$$

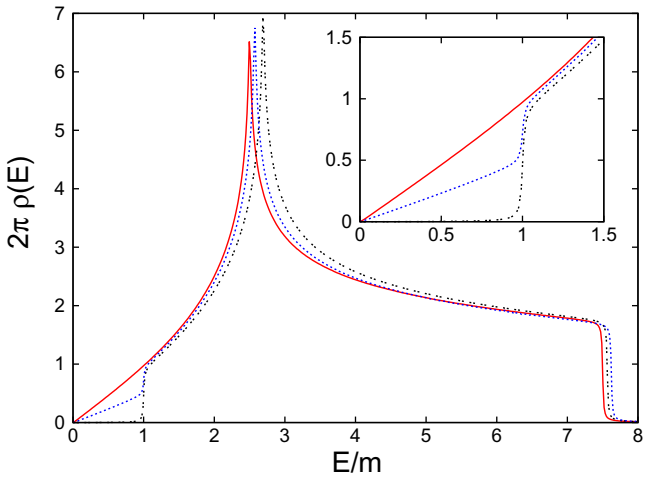

Figure 5. DOS of the full tight-binding model is evaluated. Solid (red) line corresponds to gapless graphene; dashed (black) line is the DOS of the model with uniform gap ($|h_3| = m = 0.4t, t' = 0$); dotted (blue) line represents the DOS of the model for nonuniform gap ($t' \neq 0$) with the same m. The inset shows the same curves for small energies. The van Hove singularity for gapless graphene lies at the hopping energy $E = t$. The shifting of the positions of the van Hove singularity as well as the change in the slopes at low energies should be noticed upon a change of the parameters m and t'.

which gives after integration in the limit $\lambda \to \infty$

$$\rho(E) = \frac{E}{2\pi} \left[\Theta(E - |m|) - \Theta(-E - |m|)\right]. \tag{18}$$

This means that there are no states with nonzero energy for $-|m| \leqslant E \leqslant |m|$, where m is the effective gap determined by the value of h_3 at the gapped valley. For the case of gapless graphene, i.e. for $M = t' = 0$, equation (18) reduces to

$$\rho(E) = \frac{E}{2\pi} \left[\Theta(E) - \Theta(-E)\right] = \frac{|E|}{2\pi}. \tag{19}$$

The evaluation of the DOS for the model with the full spectrum and both uniform and nonuniform gap (i.e. with $|h_3| = m$) can be performed numerically, since the integration has to be carried out over the whole BZ. The DOS of graphene for different gap realizations is shown in figure 5. For small energies, the DOS of gapless graphene shown as a (red) solid curve exhibits a linear behavior of the single Dirac cone model predicted by equation (19) (note the inset of figure 5). The DOS of the gapped model shown as a (black) dashed line is zero for energies smaller than the gap m and experiences a jump from zero to a finite value ($|m|/2\pi$ in the linear limit) at the energy $E = m$. The DOS of the model with the nonuniform gap depicted as a (blue) dotted line in figure 5 demonstrates an intermediate behavior in comparison to the other models. On the one hand, it behaves linearly for energies smaller than the gap m. But the slope of the linear asymptote is only half of the corresponding value of gapless graphene, since the number of preserved Dirac cones in the BZ is half the number of Dirac cones of the gapless model. On the other hand, the DOS also reveals a discontinuous behavior at $E = m$ where the energy becomes sufficient to allow electrons to tunnel through the potential barrier

of $2m$ that separates the valence band from the conductivity band. The position of van Hove singularity-related peaks in the DOS reveals dependence on the gap m and for $m = 0$ lies at the next-neighbor hopping energy $E = t$, as can be seen from figure 5.

4. Optical conductivities

Within the linear response approach, the conductivity tensor for Hamiltonian H is given by the Kubo formula. Then we obtain the conductivity at inverse temperature β [30],

$$\sigma_{\mu\nu}(\omega) = \frac{\mathrm{i}}{\hbar} \lim_{\alpha\to 0} \int_{\mathrm{BZ}} \sum_{l,l'=0,1} \langle k,l|j_\mu|k,l'\rangle\langle k,l'|j_\nu|k,l\rangle \frac{1}{E_{k,l}-E_{k,l'}} \frac{f_\beta(E_{k,l'})-f_\beta(E_{k,l})}{E_{k,l}-E_{k,l'}+\omega-i\alpha} \frac{\mathrm{d}^2k}{\Omega_{\mathrm{BZ}}}, \tag{20}$$

where $f_\beta(E) = 1/(1+\exp(\beta(E-E_{\mathrm{F}})))$ the Fermi–Dirac distribution at the inverse temperature β, E_{F} is the Fermi energy, and ω is the frequency of the external field. $|k,l\rangle$ is the eigenstate of H with eigenvalue $E_{k,l} = (-1)^l E_k$. The index l refers to the upper ($l = 0$) and lower ($l = 1$) band, respectively. Moreover, the current operator reads

$$j_\mu = \mathrm{i}e[H, r_\mu], \quad j_\mu = e\frac{\partial H}{\partial k_\mu}. \tag{21}$$

For the off-diagonal matrix elements with $l' \neq l$, we obtain from the Hamiltonian in equation (5)

$$\begin{aligned} &\langle k,l|j_\mu|k,l'\rangle\langle k,l'|j_\nu|k,l\rangle = \frac{p_{\mu,a}p_{\nu,b}}{E_k^2}\left(E_k^2\delta_{ab} - h_a h_b\right) + (-1)^l i\epsilon_{abc}\frac{p_{\mu,a}p_{\nu,b}h_c}{E_k}, \\ &p_{\nu,a} = \frac{\partial h_a}{\partial k_\nu}. \end{aligned} \tag{22}$$

The low-energy (Dirac) Hamiltonian, defined in equation (10) with $h_a = k_a$ ($a = 1, 2$) and $h_3 = m$, gives the following expression for the current tensor,

$$\langle k,l|j_\mu|k,l'\rangle\langle k,l'|j_\nu|k,l\rangle = e^2\left[\delta_{\mu\nu} - \frac{k_\mu k_\nu}{E_k^2} + (-1)^l i\epsilon_{\mu\nu 3}\frac{m}{E_k}\right]. \tag{23}$$

In case of the low-energy approximation, the integration over the BZ can be approximated by a circular area with radius λ. The longitudinal conductivity ($\mu = \nu$) is real due to the diagonal expression in equation (23). On the other hand, for the Hall conductivity, where $\mu \neq \nu$, the matrix element is complex,

$$\begin{aligned} &\langle k,l|j_\mu|k,l'\rangle\langle k,l'|j_\mu|k,l\rangle = e^2\frac{E_k^2 - k_\mu^2}{E_k^2}, \\ &\langle k,l|j_\mu|k,l'\rangle\langle k,l'|j_\nu|k,l\rangle = -e^2\frac{k_\mu k_\nu - (-1)^l \mathrm{i}\epsilon_{\mu\nu 3} m E_k}{E_k^2}. \end{aligned} \tag{24}$$

From the Kubo formula of equation (20), we then obtain for the real part of the conductivity

$$\sigma'_{\mu\mu}(\omega) = \frac{e^2}{\hbar}\int_0^\lambda \frac{E_k^2+m^2}{8E_k^3}\left[f_\beta(E_k) - f_\beta(-E_k)\right]\left[\delta(\omega-2E_k)+\delta(\omega+2E_k)\right]k\,\mathrm{d}k. \tag{25}$$

Finally, taking spin and valley degeneracy into account (factor 4) and sending $\lambda \to \infty$, we obtain [31, 32]

$$\sigma'_{\mu\mu}(\omega) = \frac{\pi e^2}{2h}\left(1 + \frac{(2m)^2}{\omega^2}\right)\left[f_\beta(\omega/2) - f_\beta(-\omega/2)\right]\left[\Theta(\omega-2m)+\Theta(-\omega-2m)\right], \tag{26}$$

which can be expressed as a function of three dimensionless variables as

$$\sigma'_{\mu\mu}(\omega) = \frac{\pi e^2}{2h} f(\beta m, \beta\mu, \beta\omega). \tag{27}$$

Hence, the longitudinal optical conductivity vanishes for $|\omega| < 2|m|$ and is nonzero for $|\omega| \geqslant 2|m|$. For zero temperature, the Fermi functions can be replaced by Heaviside step functions $\lim_{\beta\to\infty} f_\beta(\pm\omega) = \Theta(\pm\omega)$ and we obtain the ac-conductivity the well-known result [31, 32]

$$\sigma'_{\mu\mu}(\omega) = \frac{\pi e^2}{2h}, \tag{28}$$

for frequencies within the electronic bands. This value has been found to be very robust and barely dependent on the temperature or quality of the sample.

One of the motivations for this work was to study the Hall conductivity in case of a broken valley symmetry, where we have a gapped and a gapless valley. Using the off-diagonal current tensor of equation (24), the integration over the BZ is approximated again by the low-energy Hamiltonian. For a uniform gap (i.e. for $t' = 0$), the rotational symmetry of the problem is restored and therefore the contribution of $k_\mu k_\nu$ in the off-diagonal current tensor vanishes. Thus, after sending the cut off $\lambda \to \infty$, we get

$$\sigma_{\mu\nu}(\omega) = -\epsilon_{\mu\nu 3} \frac{e^2}{\hbar} \frac{m}{4\pi} \int_{|m|}^{\infty} \left[f_\beta(E) - f_\beta(-E)\right] \left(\frac{1}{\omega - 2E - \mathrm{i}0^+} - \frac{1}{\omega + 2E - \mathrm{i}0^+}\right) \frac{\mathrm{d}E}{E}. \tag{29}$$

For $|E_\mathrm{F}| \leqslant |m|$ and $T = 0$, the integral gives

$$\sigma'_{\mu\nu}(\omega) = \epsilon_{\mu\nu 3} \frac{m}{4\pi\omega} \log\left|\frac{2m + \omega}{2m - \omega}\right|. \tag{30}$$

At frequency $\omega = 2m$, there is a logarithmic divergence in the Hall conductivity. For large frequencies, ω, this expression approaches zero, while for any nonzero gap and $\omega \to 0$, it approaches the constant value that depends only on the sign of m,

$$\sigma'_{12} \approx \frac{m}{4\pi|m|} \frac{e^2}{\hbar} = \frac{\mathrm{sgn}(m)}{2} \frac{e^2}{h}. \tag{31}$$

These are the well-known Hall plateaux of Dirac fermions $\pm e^2/h$ [17]. This result implies for two valleys with gap parameters m and m' [16]

$$\sigma'_{12} \approx \left[\mathrm{sgn}(m) - \mathrm{sgn}(m')\right] \frac{e^2}{2h}. \tag{32}$$

5. Discussion and conclusions

An evaluation of the DOS (equation (16)), the longitudinal conductivity and the Hall conductivity (equations (20) and (22)) are performed numerically for the full tight-binding spectrum. The results are presented in figures 5–7 as a function of energy (DOS) or as functions of frequency (conductivities) for nonzero temperatures. We compare the situation without spin texture ($t' = 0$), both for the gapless case $m = 0$ and the uniform gap $m \neq 0$ and the situation with spin texture ($t' \neq 0$). In the latter, we fix the Berry phase by $\phi = -\pi/4$ and the uniform gap parameter by $M = 3t'(1 + \sqrt{3})/\sqrt{2}$ and call this the asymmetric valley, whereas the case $t' = 0$ is the symmetric valley.

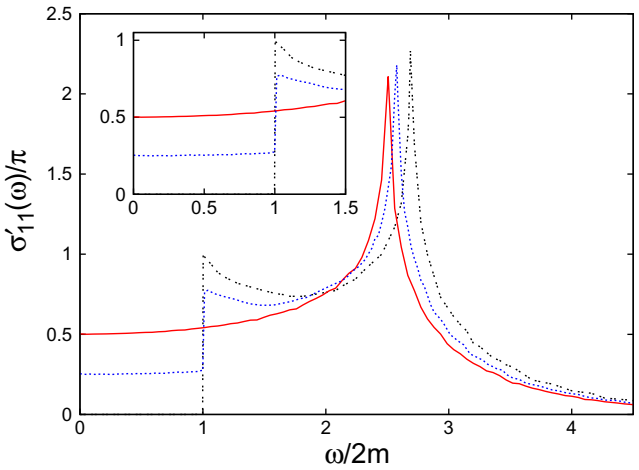

Figure 6. Real part of the longitudinal optical conductivity at half-filling for $T = 0\,K$ and $m = 0.4t$ in units of e^2/h. Here, we show optical conductivities for (a) gapless graphene (red solid line); (b) the model with uniform gap (black dashed line); (c) the model with nonuniform gap (blue dotted line). The inset shows the same curves for small frequencies. Positions of the van Hove related peaks coincide with those of the DOS if one relates frequencies to the energies from figure 5 by $\omega = 2E$.

DOS. The effect of the periodic magnetic flux, as described by h_3 in equation (15), is reflected by the DOS in figure 5. There is either a full gap (symmetric valleys) or a gapless DOS (asymmetric valley). The DOS of the asymmetric valley has a reduced slope in comparison with the case where both valleys are gapless ($M = t' = 0$), since only one valley contributes at low energies. The position of the van Hove singularity depends on the parameters M, t' and moves to higher energies as we switch on M and t'.

Longitudinal conductivity. The behavior of the longitudinal optical conductivity in figure 6 for $M = t' = 0$ reproduces the constant universal value $\sigma'_{\mu\mu} = \pi e^2/2h$ at low frequencies. At higher frequencies, it increases due to the van Hove singularity, just like the DOS. This is also the case for $M \neq 0$, where the gap for $t' = 0$ leads to a vanishing conductivity for frequencies less than the gap width $\Delta = 2m$ and jumps to higher values than the gapless conductivity at $\omega = 2m$. For the asymmetric valleys, the conductivity behaves similarly, with the conductivity reduced by a factor $1/2$ inside the gap though.

Hall conductivity. The form of h_3 in equation (15) allows us to change the gap parameter at the two valleys separately. This means that the Hall conductivities of the two valleys either subtract each other (for $\mathrm{sgn}(h_{3,1}) = \mathrm{sgn}(h_{3,2})$) or add each other (for $\mathrm{sgn}(h_{3,1}) = -\mathrm{sgn}(h_{3,2})$), when $h_{3,j}$ is the gap parameter at valley j (cf equation (32)). The reason is that the Hall conductivities can be evaluated at each gapped valley separately, using the low-energy result of equation (31). Thus, for the asymmetric valleys, where one valley is gapped and the other is gapless, we have only a contribution of $e^2\,\mathrm{sgn}(m)/2h$ from the gapped valley. This is what we see at low frequencies in figure 7. Moreover, there is a logarithmic singularity at $\omega = 2m$. It is not related to the van Hove singularity but appears when the frequency of the external field reaches the gap energy. Apparently, the optical Hall conductivity increases dramatically as the states at the edge of the gap start to contribute to transport [33]. The position of this singularity

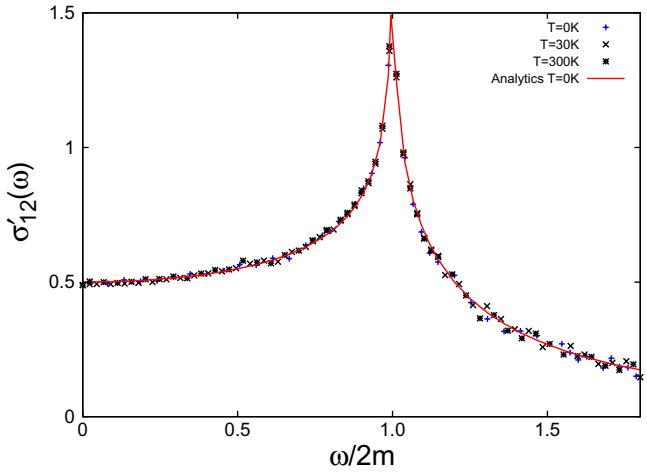

Figure 7. Real part of the optical Hall conductivity at half-filling for $T = 0, 30$ and 300 K in units of e^2/h. Numerical results calculated for the full tight-binding model (dots and crosses) and compared with the low-energy approximation of equation (30) (red solid line).

is quite robust and only determined by the gapwidth, in contrast to the parameter-dependent position of the van Hove singularity. In particular, the properties of the optical Hall conductivity do not change over a wide range of temperatures (cf figure 7). This remarkable effect can be used to measure the gap within a transport measurement. This offers an alternative to other methods of measuring spectral properties through transport properties [34].

Our transport calculation is based on the assumption that the spin texture is rigid and translationally invariant on one sublattice. This is not realistic because a 2D structure cannot have a stable order. Consequently, there will always be fluctuations, similar to the geometric fluctuations of the graphene sheet itself in the form of ripples [35]. Spin fluctuations, although with long-ranged correlations at low temperatures, lead to fluctuations in the effective magnetic flux experienced by the electrons in our model. These fluctuations appear as a σ_3 term in the Hamiltonian of equation (5), whereas fluctuations due to ripples are associated with $\sigma_{1,2}$ terms [36, 37]. Therefore, ripples may not affect the gap structure in our model, in contrast to spin fluctuations. If the latter are strong, it is possible that the effective gap, relevant to the transport properties, will be closed [38]. This may lead to a vanishing Hall conductivity. On the other hand, weak spin fluctuations may not close the gap such that the transport properties are only weakly affected. In particular, the Hall conductivity is very robust against fluctuations, as our result for thermal fluctuations in figure 7 demonstrates.

Recent experiments for sublattice-symmetry breaking by hydrogen atoms in graphene have revealed that the gap formation is not a problem even when ripples and defects are present [3]. Since the gap in our model is also created by sublattice-symmetry breaking (due to next-nearest-neighbor hopping t'), we expect a similar robustness of the gap here. The main effect of the spin texture is to break the valley symmetry. For this to be seen, it is probably sufficient to have some anisotropy in a fluctuating spin texture.

There are several other possible mechanisms for a gap formation such as boundary effects, electron–phonon interaction, Coulomb interaction and spin–orbit coupling. They may not be relevant here because of their weakness in comparison with the next-nearest-neighbor hopping

created by the doping atoms. This view is supported by a number of experiments on pristine graphene [1, 2], where no gap was observed.

In conclusion, we have suggested a possible valley symmetry breaking by a periodic magnetic flux. The latter is generated by doping of the graphene sheet with spin 1/2 atoms. The periodic flux opens gaps at both valleys whose values can be controlled independently. However, in contrast to a homogeneous magnetic field, it does not create Landau levels. Consequently, at most, two Hall plateaux can be observed. Our calculations have revealed that a gap $\Delta = 2|m|$ in both valleys creates the usual Hall plateaux with $\sigma_{12} = e^2/h$ when the gap parameter has opposite signs at the two valleys but a vanishing Hall conductivity if the signs of m are equal. The Hall conductivity is $\sigma_{12} = e^2/2h$ if one valley is gapped and the other is gapless. Moreover, the optical Hall conductivity has a logarithmic singularity when the frequency of the external microwave field reaches the gap energy. This singularity is very robust and should be visible even at room temperature. Therefore, it can be used for an accurate determination of the gap by measuring the optical properties of graphene.

Acknowledgment

We acknowledge financial support from DFG grant no. ZI 305/5-1.

References

[1] Novoselov K S *et al* 2004 *Science* **306** 5696
[2] Novoselov K S *et al* 2006 *Nat. Phys.* **2** 177
[3] Elias D C *et al* 2009 *Science* **323** 610
[4] Ohta T *et al* 2006 *Science* **313** 951
[5] Castro E V *et al* 2007 *Phys. Rev. Lett.* **99** 216802
[6] Min H *et al* 2007 *Phys. Rev.* B **75** 155115
[7] Oostinga J B *et al* 2008 *Nat. Mater.* **7** 151
[8] Zhang Y *et al* 2009 *Nature* **459** 820
[9] Mak K F *et al* 2009 *Phys. Rev. Lett.* **102** 256405
[10] Zhou S Y *et al* 2007 *Nat. Mater.* **6** 770
[11] Gietz I *et al* 2008 *Nano Lett.* **8** 4603
[12] Zhou S Y *et al* 2008 *Phys. Rev. Lett.* **101** 086402
[13] Bangert U *et al* 2010 *Phys. Rev.* B **81** 245423
[14] Coletti C *et al* 2010 *Phys. Rev.* B **81** 235401
[15] McChesney J L *et al* 2010 *Phys. Rev. Lett.* **104** 136803
[16] Haldane F D M 1988 *Phys. Rev. Lett.* **61** 2015
[17] Semenoff G 1984 *Phys. Rev. Lett.* **53** 2489
[18] Xiao D *et al* 2007 *Phys. Rev. Lett.* **99** 236809
[19] Zhang C *et al* 2009 *Phys. Rev.* B **79** 245424
[20] Yao W *et al* 2008 *Phys. Rev.* B **77** 235406
[21] Stankovich S *et al* 2006 *Nature* **442** 282
[22] Ruoff R 2008 *Nat. Nanotechnol.* **3** 10
[23] Duplock E J *et al* 2004 *Phys. Rev. Lett.* **92** 225502
Duplock E J *et al* 2008 *Nano Lett.* **8** 4597
[24] Zener C 1951 *Phys. Rev.* **82** 403
[25] Anderson P W and Hasegawa H 1955 *Phys. Rev.* **100** 675

[26] de Gennes P G 1960 *Phys. Rev.* **118** 141
[27] Müller-Hartmann E and Dagotto E 1996 *Phys. Rev.* B **54** R6819
[28] Murakami S and Nagaosa N 2000 *Phys. Rev.* B **62** R6065
[29] Campana I *et al* 2006 *Phil. Mag.* **86** 1667
[30] Ziegler K 2006 *Phys. Rev. Lett.* **97** 266802
[31] Gusynin V P *et al* 2007 *Phys. Rev.* B **75** 165407
[32] Ziegler K 2007 *Phys. Rev.* B **75** 233407
[33] Hill A *et al* 2011 arXiv:1005.3211 in preparation
[34] Zhang L M *et al* 2008 *Phys. Rev.* B **78** 235408
[35] Meyer J C *et al* 2007 *Nature* **446** 60
[36] Castro Neto A H *et al* 2009 *Rev. Mod. Phys.* **81** 109
[37] Abergel D S L *et al* 2010 *Adv. Phys.* **59** 261
[38] Ziegler K 2009 *Phys. Rev. Lett.* **102** 126802
Ziegler K 2009 *Phys. Rev.* B **79** 195424